






Attempts to produce new americium isotopes near $N = 126$

L. Ma (马龙) ¹, H. B. Yang (杨华彬) ^{1,*}, Z. Y. Zhang (张志远)^{1,2}, J. C. Pei (裴俊琛)³, M. H. Huang (黄明辉)¹, M. M. Zhang (张明明)¹, C. Y. Qiao (乔春源)³, X. J. Bao (包小军)⁴, Y. L. Tian (田玉林)¹, C. L. Yang (杨春莉)¹, Y. S. Wang (王永生)^{1,2,5}, Z. Zhao (赵圳)^{1,2}, X. Y. Huang (黄鑫源)^{1,2}, S. Y. Xu (徐苏扬) ^{1,2}, W. X. Huang (黄文学) ^{1,2}, Z. Liu (刘忠)^{1,2}, X. H. Zhou (周小红)^{1,2}, and Z. G. Gan (甘再国) ^{1,2}

¹CAS Key Laboratory of High Precision Nuclear Spectroscopy, Institute of Modern Physics, Chinese Academy of Sciences, Lanzhou 730000, China

²School of Nuclear Science and Technology University of Chinese Academy of Sciences, Beijing 100049, China

³State Key Laboratory of Nuclear Physics and Technology, School of Physics, Peking University, Beijing 100871, China

⁴Department of Physics, Hunan Normal University, Changsha 410081, China

⁵School of Nuclear Science and Technology Lanzhou University, Lanzhou 730000, China



(Received 1 June 2022; accepted 14 September 2022; published 21 September 2022)

Searches for new americium isotopes with neutron number around 126 are made in bombardments of $^{191,193}\text{Ir}$ targets with ^{40}Ar ions by employing the gas-filled recoil separator SHANS and the recoil- α correlation technique. No evidence for nuclides of interest is obtained, and the upper limits of the cross sections producing the evaporation residues are estimated to be 31.4 pb and 5.4 pb for the reactions of $^{40}\text{Ar} + ^{193}\text{Ir}$ and $^{40}\text{Ar} + ^{191}\text{Ir}$, respectively. We have performed microscopic finite-temperature Skyrme Hartree-Fock+ (Bardeen-Cooper-Schrieff theory) BCS calculations, and found that the fission barriers of compound nuclei in this region decrease rapidly with increasing proton number. The non-observation of new americium isotopes would be attributed to small survival probabilities of the ^{231}Am and ^{233}Am compound nuclei due to their much reduced fission barriers at high excitations.

DOI: [10.1103/PhysRevC.106.034316](https://doi.org/10.1103/PhysRevC.106.034316)

I. INTRODUCTION

In the translead region, neutron-deficient nuclides decay pervasively by emitting α particles, and hence α -decay spectroscopy is employed generally to identify new heavy isotopes and to study the decay properties of heavy nuclides. Based on the systematics of α -decay data, we can probe the limit to the isotope existence and shell structure evolution while changing proton or neutron numbers. Experimentally, it is very challenging to synthesize extremely neutron-deficient heavy nuclides due to their tiny production cross sections and short half-lives. Fortunately, with the advent of high-intensity heavy-ion accelerators together with the development of fast electronics, α -decay spectroscopy has revived in the neutron-deficient heavy mass region.

Since 2012, we have performed a series of experiments aimed at exploring the hitherto unknown region of the nuclear chart with $Z \sim 92$ and $N \sim 126$. A batch of most neutron-deficient isotopes from actinium to neptunium were produced using fusion-evaporation reactions and identified by employing the gas-filled recoil separator SHANS (Spectrometer for Heavy Atoms and Nuclear Structure) [1–8,10,15]. With plenty of α -decay data, we established the α -decay systematics for Np isotopes, and studied the robustness of the $N = 126$ shell closure and α -decay properties in the heavy mass region

[2–15]. Of particular finding is that the α -decay reduced widths of $^{214,216}\text{U}$ are abnormally enhanced as compared to those of the even-even nuclei with $N < 126$ [15]. This intriguing phenomenon is interpreted by the strong monopole interaction between the valence protons and neutrons occupying the $f_{7/2}$ and $f_{5/2}$ spin-orbit partner orbits, respectively. In the transuranium region, it is expected that valence protons occupy the $f_{7/2}$ orbit with continuously increasing probability with increasing atomic number, which could lead to further enhancement of the monopole proton-neutron interaction and consequently give rise to larger α -decay reduced widths. Therefore, it is interesting to extend the systematics of the α -decay reduced width to higher- Z nuclides. This motivates us to synthesize new americium nuclides and study their α -decay properties.

The element of americium was discovered via neutron capture on ^{239}Pu in 1944 [16]. From then on, americium isotopes with $A = 230$ and from $A = 232$ to 247 have been discovered successively, and the americium isotopic chain has been significantly expanded. Recently, Devaraja *et al.* reported that ^{223}Am and ^{229}Am were observed in multinucleon transfer reactions of $^{48}\text{Ca} + ^{248}\text{Cm}$ [17]. In the present work, we aim at synthesizing the hitherto unknown ^{226}Am , ^{227}Am , and ^{228}Am nuclides with neutron number around 126, for which the expected α -decay schemes are presented in Fig. 1. Theoretically, ^{226}Am , ^{227}Am , and ^{228}Am isotopes were predicted to decay by emitting α particles with Q_α of 9.466, 9.116, and 8.497 MeV, respectively [18]. Based

*Corresponding author: yanghb@impcas.ac.cn

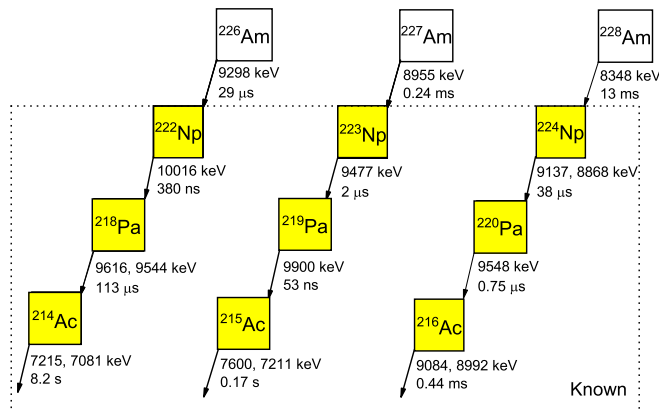


FIG. 1. Expected decay chains for ^{226}Am , ^{227}Am , and ^{228}Am . The decay schemes for their daughter nuclides are taken from Refs. [5,6,10,21,22]. The properties of ^{226}Am , ^{227}Am , and ^{228}Am are taken from the theoretical predictions [18–20].

on a new Geiger-Nuttall law proposed by Ren and Ren [19,20], the partial α -decay half-lives of ^{226}Am , ^{227}Am , and ^{228}Am were calculated to be 29 μs , 240 μs , and 13.2 ms, respectively.

II. EXPERIMENTAL DETAILS

To determine the optimal beam energies to produce the nuclides of interest, we calculated excitation functions for the $^{40}\text{Ar} + ^{193}\text{Ir}$ and $^{40}\text{Ar} + ^{191}\text{Ir}$ reactions using the statistical model code HIVAP, which is commonly used to estimate production cross sections for heavy nuclides. The parameters were adapted to reproduce the experimental data of two reactions, $^{24}\text{Mg} + ^{208}\text{Pb}$ [23] and $^{34}\text{S} + ^{198}\text{Pt}$ [24]. Results for the production of the evaporation residues in the $4n$ and $5n$ channels are displayed in Fig. 2. The calculated maximum production cross sections of ^{226}Am , ^{227}Am , and ^{228}Am are 23 pb, 70 pb, and 148 pb, respectively. Given that the nuclides of interest decay mainly by emitting α particles, it is feasible to identify them by employing a gas-filled recoil separator and the recoil- α correlation technique. It is suggested from Fig. 2 that the optimum beam energies for producing $^{227,229}\text{Am}$ via $4n$ evaporation channel and $^{226,228}\text{Am}$ via $5n$ channel are ≈ 192 and ≈ 200 MeV, respectively.

The experiments were carried at the Heavy Ion Research Facility in Lanzhou (HIRFL), China. The ^{191}Ir and ^{193}Ir targets were irradiated with ^{40}Ar ions for 190 and 60 h, respectively. An ^{40}Ar beam of ~ 300 pA intensity, at several beam energies in the range of 190–204 MeV, was supplied by the Sector-Focusing Cyclotron (SFC) of HIFRL. The $^{191,193}\text{Ir}$ targets were prepared by sputtering the enriched $^{191,193}\text{Ir}$ materials onto a 60- $\mu\text{g}/\text{cm}^2$ -thick carbon foil. The thickness of ^{193}Ir and ^{191}Ir targets were 360 $\mu\text{g}/\text{cm}^2$ and 410 $\mu\text{g}/\text{cm}^2$, respectively. The targets were mounted on a rigid frame which moved horizontally and periodically from side to side during the beam irradiation to inhibit the target breaking due to the beam heating. A total of 1.28×10^{18} and 4.05×10^{17} ions were delivered onto the 191 and ^{193}Ir targets, respectively.

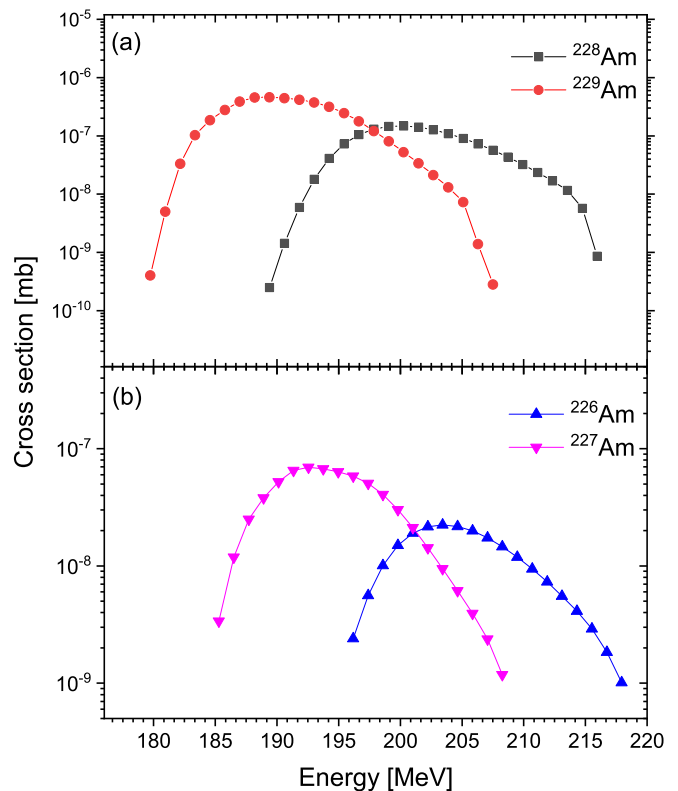


FIG. 2. (a) Excitation functions calculated using HIVAP for production of $^{228,229}\text{Am}$ nuclides in the reaction $^{40}\text{Ar} + ^{193}\text{Ir}$. (b) for $^{226,227}\text{Am}$ isotopes in the reaction $^{40}\text{Ar} + ^{191}\text{Ir}$.

The evaporation residues (ERs) recoiling out from the target foil were separated from the primary beam particles and other unwanted reaction products by using the gas-filled recoil separator SHANS, which was filled with helium gas at a pressure of 0.6 mbar. The filtered ERs were implanted into three position-sensitive 16-strip detectors (PSSDs), which were mounted side by side at the focal plane of SHANS. To detect the α particles escaping from the PSSDs, eight side silicon detectors (SSDs) were placed perpendicular to the surface of PSSDs in an open box geometry. The energy, position, and time of the implantation of ERs and their subsequent α -decay events were measured using these detectors. The total detection efficiency of the detector array was measured to be 72%. In order to distinguish the α -decay events from the implantation ones, two multiwire proportional counters were mounted upstream from the PSSDs. Behind the PSSDs, three punch-through silicon detectors were mounted for the rejection of signals produced by energetic light particles. All the detectors were cooled down to a temperature of 251 K through circulating alcohol. Signals from all the preamplifiers of detection system were processed by a digital data acquisition system, which consists of 16 waveform digitizers V1724 from CAEN S.P.A [25]. The shapes of the signals from PSSDs were recorded in 30- μs -long traces with 100 MHz sampling frequency. In the subsequent off-line analysis, the time and energy information stored in the traces were extracted using the digital triangular algorithm [26] and pulse shape fitting method [27], respectively.

Energy calibrations of the PSSDs and SSDs were initially made using a mixed α source of ^{239}Pu , ^{241}Am , and ^{244}Cm , which emit α particles with energies in the range of 5–6 MeV. Additionally, the detectors were calibrated by using the dominant α -decay peaks from the known nuclides produced in the irradiation with a ^{175}Lu target. The typical energy resolution for the PSSDs was 40 keV [full width at half-maximum (FWHM)] for 6.5–10 MeV α particles fully absorbed in the PSSDs, while the reconstructed α lines for the escaping α particles, recorded by the PSSDs and SSDs together, had an energy resolution of 100–180 keV (FWHM) for 7.5–MeV α activity. A systematic uncertainty of 15 keV was taken into account in the calculation of energy errors. The vertical position resolution (FWHM) of the PSSDs was better than 1.5 mm for $ER - \alpha$ correlated events.

III. EXPERIMENTAL RESULTS AND DISCUSSION

The identification of rare activities of interest was performed by searching for correlated α -decay chains. It was required that an implant and its subsequent three successive decays ($\alpha 1$, $\alpha 2$, and $\alpha 3$) occurred in the same place of the PSSDs, within a 1.5-mm-wide vertical position window, and that all signals (implant plus three decays) were registered within a 12-s period. The searching time windows were set to be $\Delta t(ER - \alpha 1) < 10$ s, $\Delta t(\alpha 1 - \alpha 2) < 1$ s, and $\Delta t(\alpha 2 - \alpha 3) < 100$ ms. In addition, we searched for pileup events with energies of 7–25 MeV using the shape fitting method [27]. However, no candidate decay chains that could be assigned to the isotopes of element americium, as shown in Fig. 1, were observed in our experiment. If the α decay of a nuclide occurred in flight through the separator, we could still observe the decay chain of its daughter nuclide. Furthermore, a somewhat surprising fact was that the products of the αxn channels were not observed either in the present work, for which the cross sections are expected to be significantly larger than those produced in the pure xn channels according to the predictions of the code HIVAP. In our previous work, large ratios between the αxn and pure neutron evaporation residues were observed experimentally [2–8,10].

The transport efficiency of SHANS was estimated to be 14% by using the reaction $^{40}\text{Ar} + ^{175}\text{Lu}$ [1], which is roughly similar to the reactions with ^{191}Ir and ^{193}Ir targets. Therefore, it is reasonable to assume that the transport efficiencies for the products of the reactions employed in the present work are about 14%. Taking into account the target thickness, total beam does deposited and transport efficiency, the upper limits of the cross sections producing the evaporation residues are estimated to be 31.4 pb and 5.4 pb for the reactions $^{40}\text{Ar} + ^{193}\text{Ir}$ and $^{40}\text{Ar} + ^{191}\text{Ir}$, respectively. The limits determined experimentally are considerably lower than those predicted by HIVAP.

In our previous work, $^{40}\text{Ar} + ^{185,187}\text{Re}$ [8,10,28] and $^{40}\text{Ar} + ^{180,182,183,186}\text{W}$ reactions [3,4,9,11,13,14] were successfully used for synthesis of new $^{220,222}\text{Np}$ and $^{215,216}\text{U}$ isotopes, and detailed α -decay studies of $^{218,219}\text{U}$, ^{222}Pa , and ^{218}Ac . For the reactions with ^{40}Ar projectiles including those used presently, Coulomb repulsive forces between the colliding nuclei are small and almost same. After projectile

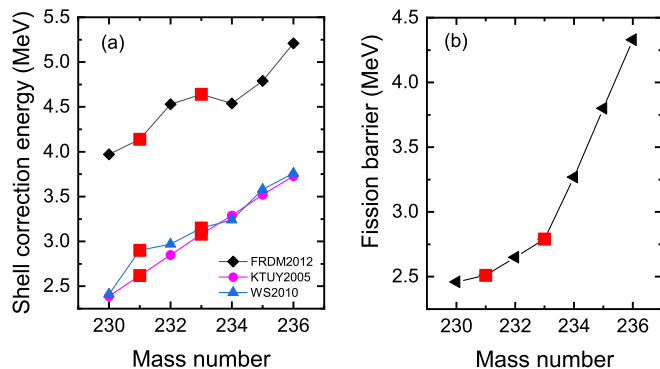


FIG. 3. (a) Evaluated shell correction energies of $^{230-236}\text{Am}$ nuclei using available theoretical models [35–37]. (b) Fission barriers of $^{230-236}\text{Am}$ nuclei obtained from FRDM [38]. The values for $^{231,233}\text{Am}$ nuclei are marked by red square.

capture onto the target nuclide, the composite system evolves similarly towards fused compound system [29–34]. In other words, the entrance channels are nearly same, and do not affect very much the fusion cross sections. Therefore, the lower residue cross sections of the $^{40}\text{Ar} + ^{193}\text{Ir}$ and $^{40}\text{Ar} + ^{191}\text{Ir}$ reactions might not be due to a slight charge-number increase of the target nuclei from 74 (W) to 77 (Ir). It would result from a sharp change in nuclear properties of extremely neutron-deficient americium compound nuclei.

Figure 3(a) presents the shell correction energies of $^{230-236}\text{Am}$ nuclei, which are derived from available theoretical models including FRDM2012, KTUY2005, and WS2010 [35–37]. In general, the shell correction energies decrease with decreasing neutron number. The fission barriers of $^{230-236}\text{Am}$ nuclei obtained from FRDM are shown in Fig. 3(b) [38]. It can be seen that the fission barrier decreases with decreasing neutron number, and the fission barriers of ^{231}Am and ^{233}Am , which are the compound nuclei produced in the $^{40}\text{Ar} + ^{193}\text{Ir}$ and $^{40}\text{Ar} + ^{191}\text{Ir}$ complete fusion reactions, are as small as 2.51 and 2.79 MeV, respectively. As a consequence, the compound nuclei would de-excite predominantly via fission, leading to very small survival probabilities of compound nuclei ^{231}Am and ^{233}Am . Therefore, the nonobservation of the nuclei of interest could be attributed to the small survival probabilities of the compound nuclei.

In order to gain a deep insight into the unexpected small production cross sections, we have performed microscopic finite-temperature Skyrme Hartree-Fock+ (Bardeen-Cooper-Schrieffer theory) BCS calculations of the fission barriers while changing excitation energy of the compound nuclei [39,40]. The Skyrme force used in this work is SkM* [41]. The calculations are carried out using the SkyAx solver [42]. The microscopic calculations can self-consistently describe the energy-dependent fission barriers in terms of free energies, and there is no need to consider additional shell effects. Figure 4 shows the fission barrier heights as a function of excitation energy of compound nuclei ^{227}Np , ^{226}U , ^{231}Am , and ^{233}Am . Indeed, it can be seen that ^{231}Am and ^{233}Am have much reduced fission barrier heights compared to those of ^{227}Np and ^{226}U . The fission barriers decrease significantly

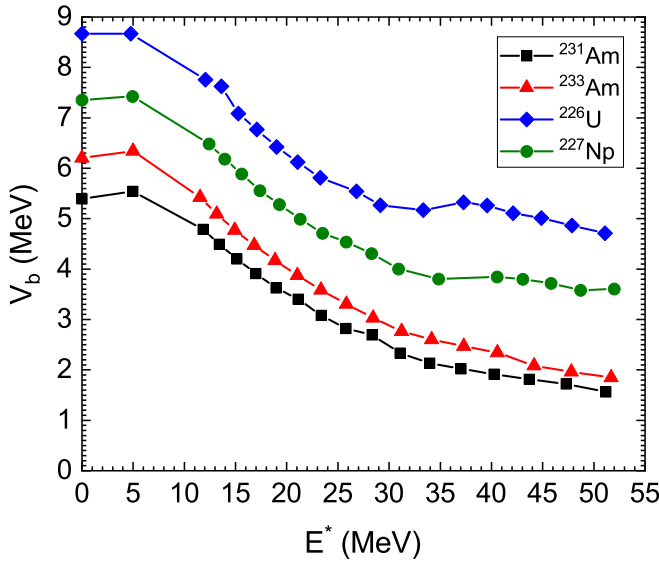


FIG. 4. Fission barrier heights of compound nuclei ^{227}Np , ^{226}U , ^{231}Am , and ^{233}Am as a function of excitation energy, calculated by the microscopic finite-temperature Skyrme Hartree-Fock+BCS approach. Please note that the excitation energies of the compound Am nuclei at the beam energies of ≈ 192 and ≈ 200 MeV are about 43 and 53 MeV, respectively.

with increasing proton number. In addition, ^{231}Am has lower fission barriers than that of ^{233}Am , showing that fission barrier also decreases with decreasing neutron number in this mass region.

We calculated the fission barrier distribution along the fission pathway of the compound nuclei. Figure 5 displays the fission barriers of ^{227}Np , ^{226}U , ^{231}Am , and ^{233}Am at an excitation energy around 50 MeV corresponding to a temperature

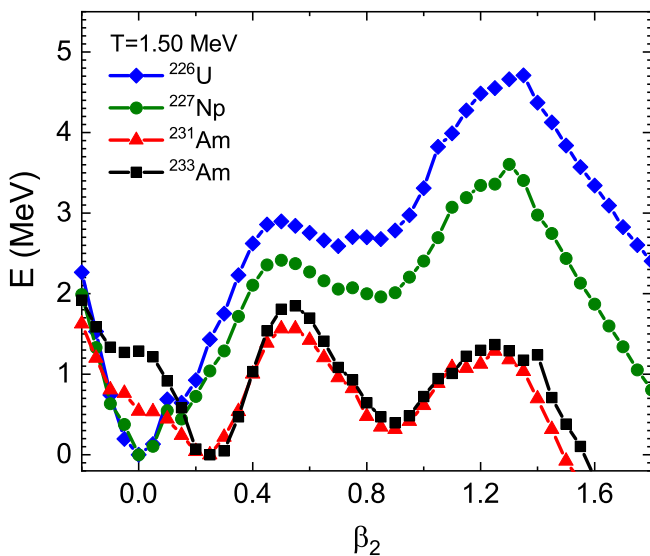


FIG. 5. Fission barrier along the fission pathway of ^{227}Np , ^{226}U , ^{231}Am , and ^{233}Am compound nuclei as a function of quadrupole deformation β_2 at an excitation energy around 50 MeV corresponding to a temperature at $T = 1.5$ MeV.

at $T = 1.5$ MeV. The fission barriers are shown as a function of quadrupole deformation β_2 . We see that, for ^{227}Np and ^{226}U , the second barriers are higher than the first ones. The significant second fission barrier is the main reason for their enhanced stability against fission. On the other hand, the second barriers in ^{231}Am and ^{233}Am are lower than the first ones, which imply that the Am compound nuclei are more inclined to fission. Note that the second barriers could be lower due to asymmetric fission, and then this has been taken into account in our calculations. In Fig. 5, we can also see that the shapes at equilibria of ^{227}Np and ^{226}U are spherical, while their ground-state shapes are around $\beta_2 = 0.22$, which demonstrates the shape phase transition [43]. The fission barrier heights can be slightly increased as a result of the shape phase transition. This is consistent with the nonmonotonic trends of fission barrier heights of ^{227}Np and ^{226}U as shown in Fig. 4. The nuclear shape phase transition [43] occurs generally at sufficient high excitations, but it is relatively delayed for ^{231}Am and ^{233}Am .

With the obtained fission barriers, we also calculated first neutron-evaporation survival probabilities of compound nuclei ^{227}Np , ^{226}U , ^{231}Am , and ^{233}Am with statistical models. In the calculations, the curvatures of the fission barriers are considered. This approach has been used for studying survival probabilities of superheavy nuclei and the details are given in Ref. [40]. The obtained first neutron-evaporation survival probabilities of ^{227}Np and ^{226}U are higher than those of $^{231,233}\text{Am}$ by at least one order of magnitude. The results imply that the residue cross sections of Am isotopes would be extremely small compared to those produced in lighter reaction systems, if taking into account multiple neutron evaporations. We are still developing the approach to calculate survival probabilities after multiple neutron evaporations based on microscopic energy-dependent fission barriers.

IV. SUMMARY

We have searched for new neutron-deficient americium isotopes employing the gas-filled recoil separator SHANS and the recoil- α correlation method. Unfortunately, no evidence for the nuclides of interest was found. The neighboring known nuclides, which can be produced in charged-particle evaporation channels, were also not observed. The upper limits of the cross sections for the evaporation residues are estimated to be 31.4 pb and 5.4 pb for the $^{40}\text{Ar} + ^{193}\text{Ir}$ and $^{40}\text{Ar} + ^{191}\text{Ir}$ reactions, respectively. The unexpected low production cross sections have been discussed on the basis of various theoretical models, and the nonobservation of new Am isotopes is likely due to the much reduced survival probabilities of compound nuclei $^{231,233}\text{Am}$ since their fission barriers are quite low at high excitations.

ACKNOWLEDGMENTS

The authors would like to thank the accelerator crew of HIRFL for providing the stable ^{40}Ar beam. This work was partially supported by the National Key R&D Program of China (Contract No. 2018YFA0404402), the Strategic Priority Research Program of Chinese Academy of Sciences (Grant No. XDB34010000), the National Natural Science

Foundation of China (Grant Nos. U1932139, 11975279, 12105328, 12075286, 11961141004, 12135004, 11635003), the Key Research Program of the Chinese Academy of Sciences (Grant No. ZDBS-LY-SLH017), the CAS project for Young Scientists in Basic Research (Grant No. YSBR-002),

the Guangdong Major Project of Basic and Applied Basic Research (Grant No. 2021B0301030006), the Youth Innovation Promotion Association CAS (Grant No. 2020409), the Special Research Assistant Grant of Chinese Academy of Sciences (Grant No. E129251Y).

-
- [1] Z. Y. Zhang, L. Ma, Z. G. Gan, M. H. Huang, T. H. Huang, G. S. Li, X. L. Wu, G. B. Jia, L. Yu, H. B. Yang, Z. Y. Sun, X. H. Zhou, H. S. Xu, and W. L. Zhan, *Nucl. Instrum. Methods Phys. Res. B* **317**, 315 (2013).
- [2] Z. Y. Zhang, Z. G. Gan, L. Ma, L. Yu, H. B. Yang, T. H. Huang, G. S. Li, Y. L. Tian, Y. S. Wang, X. X. Xu, X. L. Wu, M. H. Huang, C. Luo, Z. Z. Ren, S. G. Zhou, X. H. Zhou, H. S. Xu, and G. Q. Xiao, *Phys. Rev. C* **89**, 014308 (2014).
- [3] L. Ma, Z. Y. Zhang, Z. G. Gan, H. B. Yang, L. Yu, J. Jiang, J. G. Wang, Y. L. Tian, Y. S. Wang, S. Guo, B. Ding, Z. Z. Ren, S. G. Zhou, X. H. Zhou, H. S. Xu, and G. Q. Xiao, *Phys. Rev. C* **91**, 051302(R) (2015).
- [4] H. B. Yang, Z. Y. Zhang, J. G. Wang, Z. G. Gan, L. Ma, L. Yu, J. Jiang, Y. L. Tian, B. Ding, S. Guo, Y. S. Wang, T. H. Huang, M. D. Sun, K. L. Wang, S. G. Zhou, Z. Z. Ren, X. H. Zhou, H. S. Xu, and G. Q. Xiao, *Eur. Phys. J. A* **51**, 88 (2015).
- [5] M. D. Sun, Z. Liu, T. H. Huang, W. Q. Zhang, J. G. Wang, X. Y. Liu, B. Ding, Z. G. Gan, L. Ma, H. B. Yang, Z. Y. Zhang, L. Yu, J. Jiang, K. L. Wang, Y. S. Wang, M. L. Liu, Z. H. Li, J. Li, X. Wang, H. Y. Lu *et al.*, *Phys. Lett. B* **771**, 303 (2017).
- [6] T. H. Huang, W. Q. Zhang, M. D. Sun, Z. Liu, J. G. Wang, X. Y. Liu, B. Ding, Z. G. Gan, L. Ma, H. B. Yang, Z. Y. Zhang, L. Yu, J. Jiang, K. L. Wang, Y. S. Wang, M. L. Liu, Z. H. Li, J. Li, X. Wang, H. Y. Lu *et al.* *Phys. Rev. C* **98**, 044302 (2018).
- [7] H. B. Yang, L. Ma, Z. Y. Zhang, C. L. Yang, Z. G. Gan, M. M. Zhang, M. H. Huang, L. Yu, J. Jiang, Y. L. Tian, Y. S. Wang, J. G. Wang, Z. Liu, M. L. Liu, L. M. Duan, S. G. Zhou, Z. Z. Ren, X. H. Zhou, H. S. Xu, G. Q. Xiao *et al.*, *Phys. Lett. B* **777**, 212 (2018).
- [8] Z. Y. Zhang, Z. G. Gan, H. B. Yang, L. Ma, M. H. Huang, C. L. Yang, M. M. Zhang, Y. L. Tian, Y. S. Wang, M. D. Sun, H. Y. Lu, W. Q. Zhang, H. B. Zhou, X. Wang, C. G. Wu, L. M. Duan, W. X. Huang, Z. Liu, Z. Z. Ren, S. G. Zhou, and Y. A. N. Polyakov, *Phys. Rev. Lett.* **122**, 192503 (2019).
- [9] M. M. Zhang, Y. L. Tian, Y. S. Wang, X. H. Zhou, Z. Y. Zhang, H. B. Yang, M. H. Huang, L. Ma, C. L. Yang, Z. G. Gan, J. G. Wang, H. B. Zhou, S. Huang, X. T. He, S. Y. Wang, W. Z. Xu, H. W. Li, X. X. Xu, L. M. Duan, Z. Z. Ren *et al.* *Phys. Rev. C* **100**, 064317 (2019).
- [10] L. Ma, Z. Y. Zhang, Z. G. Gan, X. H. Zhou, H. B. Yang, M. H. Huang, C. L. Yang, M. M. Zhang, Y. L. Tian, Y. S. Wang, H. B. Zhou, X. T. He, Y. C. Mao, W. Hua, L. M. Duan, W. X. Huang, Z. Liu, X. X. Xu, Z. Z. Ren, S. G. Zhou *et al.*, *Phys. Rev. Lett.* **125**, 032502 (2020).
- [11] M. M. Zhang, H. B. Yang, Z. G. Gan, Z. Y. Zhang, M. H. Huang, L. Ma, C. L. Yang, C. X. Yuan, Y. S. Wang, Y. L. Tian *et al.*, *Phys. Lett. B* **800**, 135102 (2020).
- [12] M. D. Sun, Z. Liu, T. H. Huang, W. Q. Zhang, A. N. Andreyev, B. Ding, J. G. Wang, X. Y. Liu, H. Y. Lu, D. S. Hou, Z. G. Gan, L. Ma, H. B. Yang, Z. Y. Zhang *et al.*, *Phys. Lett. B* **800**, 135096 (2020).
- [13] W. Hua, Z. Zhang, L. Ma, Z. Gan, H. Yang, M. Huang, C. Yang, M. Zhang, Y. Tian, X. Zhou, C. Yuan, C. Shen, and L. Zhu, *Chin. Phys. C* **45**, 044003 (2021).
- [14] W. Hua, Z. Zhang, L. Ma, Z. Gan, H. Yang, C. Yuan, M. Huang, C. Yang, M. Zhang, Y. Tian, and X. Zhou, *Chin. Phys. C* **45**, 044001 (2021).
- [15] Z. Y. Zhang, H. B. Yang, M. H. Huang, Z. G. Gan, C. X. Yuan, C. Qi, A. N. Andreyev, M. L. Liu, L. Ma, M. M. Zhang, Y. L. Tian, Y. S. Wang, J. G. Wang, C. L. Yang, G. S. Li, Y. H. Qiang, W. Q. Yang, R. F. Chen, H. B. Zhang, Z. W. Lu *et al.*, *Phys. Rev. Lett.* **126**, 152502 (2021).
- [16] G. T. Seaborg, *Chem. Eng. News Archive* **23**, 2190 (1945).
- [17] H. M. Devaraja, S. Heinz, O. Beliuskina, V. Comas, S. Hofmann, C. Hornung, G. Münzenberg *et al.*, *Phys. Lett. B* **748**, 199 (2015).
- [18] M. Bao, Z. He, Y. M. Zhao, and A. Arima, *Phys. Rev. C* **90**, 024314 (2014).
- [19] Y. Ren and Z. Ren, *Phys. Rev. C* **85**, 044608 (2012).
- [20] Y. Ren and Z. Ren, *Nucl. Sci. Tech.* **24**, 050518 (2013).
- [21] NNDC National Nuclear Data Center, Chart of Nuclides, <https://www.nndc.bnl.gov/nudat3>
- [22] A. K. Mistry, J. Khuyagbaatar, F. P. Heßberger, D. Ackermann, B. Andel, S. Antalic *et al.*, *Nucl. Phys. A* **987**, 337 (2019).
- [23] A. N. Andreyev, D. D. Bogdanov, V. I. Chepigin, A. P. Kabachenko, O. N. Malyshev, A. G. Popeko, R. N. Sagaidak, G. M. Ter-Akopian, M. Veselsky, and A. V. Yeremin, *Z. Phys. A* **347**, 225 (1994).
- [24] K. Nishio, H. Ikezoe, S. Mitsuoka, K. Satou, and C. J. Lin, *Phys. Rev. C* **68**, 064305 (2003).
- [25] V1724 & VX1724 user manual, <http://www.caen.it/csite>, 2018 (accessed 1 November 2018).
- [26] V. T. Jordanov and G. F. Knoll, *Nucl. Instrum. Methods Phys. Res.* **345**, 337 (1994).
- [27] H. B. Yang, Z. G. Gan, Z. Y. Zhang, M. M. Zhang, M. H. Huang, L. Ma, C. L. Yang *et al.*, *Eur. Phys. J. A* **55**, 8 (2019).
- [28] L. Ma, Z. Y. Zhang, H. B. Yang, M. H. Huang, M. M. Zhang, Y. L. Tian, C. L. Yang, Y. S. Wang, Z. Zhao, W. X. Huang, Z. Liu, X. H. Zhou, and Z. G. Gan, *Phys. Rev. C* **104**, 044310 (2021).
- [29] A. B. Quint, W. Reidorf, K.-H. Schmidt, P. Armbruster, F. P. Heßberger, S. Hofmann *et al.*, *Z. Phys. A* **346**, 119 (1993).
- [30] W. J. Swiatecki, *Nucl. Phys. A* **376**, 275 (1982).
- [31] S. Bjørnholm and W. J. Swiatecki, *Nucl. Phys. A* **391**, 471 (1982).
- [32] K. Satou, H. Ikezoe, S. Mitsuoka, K. Nishio, and S. C. Jeong, *Phys. Rev. C* **65**, 054602 (2002).
- [33] K. Satou, H. Ikezoe, S. Mitsuoka, K. Nishio, C. J. Lin, and S. C. Jeong, *Phys. Rev. C* **73**, 034609 (2006).
- [34] Y. T. Oganessian, in *Heavy Elements and Related New Phenomena*, edited by W. Greiner and R. K. Gupta (World Scientific, Singapore, 1999), Vol. 1, p. 43.

- [35] P. Möller, A. J. Sierk, T. Ichikawa, and H. Sagawa, *At. Data Nucl. Data Tables* **109-110**, 1 (2016).
- [36] H. Koura, T. Tachibana, M. Uno, and M. Yamada, *Prog. Theor. Phys.* **113**, 305 (2005).
- [37] N. Wang, Z. Liang, Min Liu, and X. Wu, *Phys. Rev. C* **82**, 044304 (2010).
- [38] P. Möller, A. J. Sierk, T. Ichikawa, A. Iwamoto, and M. Mumpower, *Phys. Rev. C* **91**, 024310 (2015).
- [39] Y. Zhu and J. C. Pei, *Phys. Rev. C* **94**, 024329 (2016).
- [40] C. Y. Qiao and J. C. Pei, *Phys. Rev. C* **106**, 014608 (2022).
- [41] J. Bartel, P. Quentin, M. Brack, C. Guet, and H. B. Hakansson, *Nucl. Phys. A* **386**, 79 (1982).
- [42] P.-G. Reinhard, B. Schuetrumpf, and J. Maruhn, *Comput. Phys. Commun.* **258**, 107603 (2021).
- [43] B. K. Agrawal, Tapas Sil, J. N. De, and S. K. Samaddar, *Phys. Rev. C* **62**, 044307 (2000).